COMPUTER METHODS AND PROGRAMS IN BIOMEDICINE 137 (2016) 231–245

journal homepage: www.intl.elsevierhealth.com/journals/cmpb

Left ventricle segmentation in fetal echocardiography using a multi-texture active appearance model based on the steered Hermite transform

Lorena Vargas-Quintero [a,*], *Boris Escalante-Ramírez* [a], *Lisbeth Camargo Marín* [b], *Mario Guzmán Huerta* [b], *Fernando Arámbula Cosio* [c], *Héctor Borboa Olivares* [b]

[a] *Universidad Nacional Autónoma de México, Facultad de Ingeniería, C.U., Mexico D.F., Mexico*
[b] *Instituto Nacional de Perinatología, Mexico D.F., Mexico*
[c] *Centro de Ciencias Aplicadas y Desarrollo Tecnológico (CCADET), Universidad Nacional Autónoma de México, Mexico D.F., Mexico*

ARTICLE INFO

Article history:
Received 15 January 2016
Received in revised form
31 August 2016
Accepted 23 September 2016

Keywords:
Segmentation
Fetal echocardiography
Active appearance models
Hermite transform

ABSTRACT

Objective: Fetal echocardiographic analysis is essential for detecting cardiac defects at early gestational ages. Fetal cardiac function can be assessed by performing some measurements regarding the dimension and shape of the heart cavities. In this work we propose an automatic segmentation method applied to the analysis of the left ventricle in fetal echocardiography.
Methods: For segmentation of the left ventricle, we designed a novel multi-texture active appearance model (AAM) based on the Hermite transform (HT). Local orientation analysis is addressed by steering the coefficients obtained with the HT. The method basically consists of an AAM-based scheme which uses the steered HT to efficiently code texture patterns of the input image. A wider and detailed description of the image features can be obtained with this method. Compared with classic AAM methods, the segmentation performance is substantially improved with the proposed scheme. Since AAM-based approaches process local information, an automatic method is also proposed to initialize the multi-texture AAM. For this purpose, a database of pre-segmented images was built. Then, techniques such as thresholding, mathematical morphology and correlation are combined to identify the position and orientation of the left ventricle. Typical issues found in fetal cardiac ultrasound images such as different orientations and shape variations of the heart cavities can be easily handled with the designed method.
Results: Several images of fetal echocardiography were used to evaluate the proposed segmentation method. The algorithm performance was validated using different metrics. We used a database of 143 real images of fetal hearts acquired for different phases of the cardiac cycle. We obtained an average Dice coefficient of 0.8631 and a point-to-curve distance of 2.027 pixels. The proposed algorithm was also validated by comparing it with other segmentation methods.
Conclusions: We have designed an automatic algorithm for left ventricle segmentation in fetal echocardiography. The reported results demonstrate that the proposed approach can achieve an efficient segmentation of the left ventricular cavity. Typical problems found in images of fetal echocardiography are satisfactorily handled with the proposed multi-texture AAM scheme.

* *Corresponding author.* Universidad Nacional Autónoma de México, Edificio de Posgrado en Ingeniería, Departamento de Procesamiento de Señales, Laboratorio Avanzado de Procesamiento de Imágenes, C.U., Mexico D.F., Mexico.
E-mail address: vargas.lorena@yahoo.com (L. Vargas-Quintero).
http://dx.doi.org/10.1016/j.cmpb.2016.09.021
0169-2607/

1. Introduction

Ultrasound is one of the most used imaging modalities for clinical applications. Ultrasound energy and acoustic properties of the body are used to build images from stationary and moving tissues. A set of pulses is emitted and amplitudes of the returning pulse-echoes are coded as gray values of the images [1]. Ultrasound systems can be used for volume measurements, anatomic distance quantification and motion evaluation. With recent advances of ultrasound systems, three and four dimensional studies can be obtained. Real time analysis can be performed with these new advances [2].

This medical imaging technique has become the standard modality for fetal evaluation. Compared with other medical imaging modalities, the most important characteristics of ultrasound systems are low cost, non-ionizing radiation, accessibility and low risk for the fetus [3,4]. Because ultrasound is also safe, painless, provides extensive and immediate results, it is a very convenient technique for fetal assessment [3,5,6]. Fetal ultrasound is frequently employed for detecting congenital diseases as well as determining the fetal age, size and gender [5–8].

Cardiac assessment is another utility of obstetrical ultrasound [5]. Evaluation of the human fetal cardiovascular system can be made using fetal echocardiographic studies. Since detection of congenital heart diseases is currently of main concern for physicians [7], analysis of the fetal heart is a fundamental task. Several tasks can be addressed to assess cardiac function: measurement of the heart stroke volume, quantification of the left and right ventricle volume at both end-diastolic and end-systolic phases [9] and motion analysis of the myocardial wall [10]. Evaluation of the fetal heart using ultrasound images requires segmenting the cardiac cavities. Manual annotation is a time consuming task which also depends on the observer. Automatic and semi-automatic algorithms are nowadays necessary tools to perform objective evaluations.

Generally speaking, the main challenges of segmenting ultrasound images are imposed by the image quality which is substantially degraded by the speckle pattern [11]. Although many efforts have been made during the last twenty years regarding the automatic segmentation of ultrasound images, the problem is still open. Moreover, the problem becomes more complicated when working with fetal cardiac ultrasound because the shape of cardiac cavities may considerably vary during different gestational ages.

Many limitations have been recognized for ultrasound systems. As mentioned, drawbacks of working with ultrasound data are related to the image quality, which is manifested in negative characteristics such as low contrast, missing contours, shadows and many other artifacts [12] that directly affect the clinical interpretation accuracy. These limitations also impact the performance of automatic segmentation algorithms.

The segmentation problem of ultrasound images has been tackled using different types of approaches [13]. Most researchers have opted for shape-based and trained models [13–17] because in these methods the segmentation is carried out within a limited range of variation which is normally defined by known shapes. These methods have demonstrated to be efficient proposals to handle the problems of ultrasound images. Segmentation of ventricular cavities has been of main interest for researchers using ultrasound images [13]. A variety of authors include prior knowledge for the heart chamber segmentation [14–19]. Hansson et al. [20] presented a segmentation model for B-mode cardiac ultrasound based on a Bayesian formulation. The method uses prior knowledge of the left ventricle and atrium position. Active contours are some of the methods that have attracted more attention to address the segmentation task in medical applications [14,16,19]. Marsousi et al. [14] proposed an adaptive method using a B-spline Snake model applied to segmentation of the left ventricle endocardial boundary in echocardiographic studies, combining external forces and employing a multiresolution strategy. Among the segmentation methods which incorporate prior knowledge, active shape models (ASMs) [15–17] and active appearance models (AAMs) [18] have demonstrated to be very efficient. They have also been used in echocardiographic images [15–18]. Classic ASMs and active contour models present many limitations in ultrasound images [15–17,19] due to the fact that they are based on edge characterization. As known, missing edges are some of the main problems of ultrasound images. In this work we adopted AAM because this method was designed to segment known shapes. It is also a good alternative to analyze not only the shape but also the object texture [21,22]. Combinations of active contours with ASM [16], graph cuts with AAM [23] and K-means with active contours [24] are other alternatives that researchers have used for segmenting cardiac ultrasound images. However, many of these techniques are very sensitive to initialization and parameter selection [25].

We propose an automatic method applied to the left ventricle segmentation using fetal echocardiography. The method consists of an AAM scheme where the left ventricle texture is modeled using the steered HT. Since AAM algorithms use image textures, we must find an efficient mechanism to represent this feature. The HT [26,27] is a mathematical tool which has been widely employed for texture coding [28]. It decomposes an image into a set of coefficients using a basis of orthogonal functions corresponding to the Hermite polynomials [26–33]. One of the most important characteristics of the HT is its ability to perform directional analysis by simply steering its coefficients [32]. It is well known that some image patterns such as edges and textures are better analyzed using directional operations [31,32]. The effectiveness of the HT as method to extract image features has also been demonstrated in several applications [29,30,33].

We then present a novel multi-texture AAM scheme for segmentation of fetal ultrasound images in which the HT advantages and its steering property are exploited. Commonly, texture modeling in classic AAMs is carried out using the original image. However, this is not the best option when working with ultrasound images due to the speckle pattern. In our scheme we incorporated the steered HT into the AAM algorithm in order to obtain a wider description of the object texture. Additionally, relevant image information of such as edges and homogeneous regions can be identified with these coefficients while preserving the cardiac cavity features. Since AAM is a local algorithm, the initialization must be good enough in order to achieve an optimal segmentation result. The design of an initialization scheme is a very challenging task because in most applications object localization may significantly vary

in the images. Even more, cardiac cavities in echocardiography may exhibit random orientations because fetuses can present different positions during an ultrasound study. To solve the initialization problem we designed a method that finds the fetal left ventricle by comparing the input image with a database of sample patches of the region of interest.

Several fetal echocardiographic images have been used for evaluating the performance of the proposed algorithm. A quantitative analysis was made using several metrics demonstrating the effectiveness of our method.

1.1. Related works

In this section we present a short review of methods that have been applied to segment the fetal heart in ultrasound images. Most of the designed approaches to segment echocardiographic images are focused on studying adult patients. Segmentation of fetal echocardiographic images is currently a hot topic. At present time, there is not much literature regarding the segmentation of fetal cardiac cavities in ultrasound data. Some of the most relevant works are focused on segmenting four cardiac cavities and the rest of them were only designed to analyze the left ventricle.

Fuzzy algorithms, active appearance models and level set methods have been used to segment fetal cardiac ultrasound images [25,34–37]. Guo et al. [25] presented a novel approach combining a sparse representation, a global constraint and a local refinement technique with active appearance models. Sampath et al. [34] proposed a fuzzy connectedness technique to segment all four chambers of the fetal heart. Image preprocessing is the first step of this approach which uses a probabilistic patch maximum likelihood estimation to reduce the speckle pattern in the ultrasound image. The fuzzy connectedness method includes reference seed points selected from the fetal cardiac structure.

Dindoyal et al. [35] employed a level set method with a prior knowledge model for fetal heart segmentation. Lassige et al. [36] also employed a level set method for delineating the endocardial borders of septal defects present in the fetal cardiac cavities. Deng et al. [37] have used an active cardiac model for segmentation of cardiac structures during early fetal ultrasound. The approach consists of a preprocessing phase where the area of interest is first located through an automatic detection based on motion estimation and anisotropic diffusion methods. Subsequently, the active cardiac model is used to describe the cardiac cavity motion.

1.2. Contributions of this work

Two main contributions are presented in this work:

- Initialization stage. We built a database which is composed of pre-segmented image examples with the most representative variations of the fetal heart region. These variations are related to orientations and scales that cardiac cavities may exhibit. Subsequently, we used a correlation operator between the input image and those of the database to detect the left ventricle position.
- Multi-texture AAM using the steered HT. We designed an AAM scheme which combines several texture maps obtained from the steered HT. With this framework, the performance of classic AAM is substantially improved. Coefficients of the steered HT are used as texture maps. We built a statistical model for each coefficient, and after they are combined using a weighted scheme.

2. Methods

2.1. AAM-based segmentation

AAM is one of the most used methods for medical image segmentation. A statistical model is obtained from a training set in this algorithm. The main objective of this technique is to code possible shape and texture variations of the structures under study. Not only the shape but also the texture is processed in AAM algorithms. In order to build the statistical model, landmarks and gray levels of the patch enclosed by landmarks are used. A finite number of training samples are needed to build the model. This technique uses prior knowledge of the structure of interest which is acquired from a training stage. This characteristic constitutes a great advantage with respect to other methods. The shape and texture vary within the range defined by the training set. Objects of interest in AAM algorithms are then described using shape points and texture. The training process is composed of three main stages: building a statistical shape model, construction of a statistical texture model and combining both statistical models. The algorithm is briefly described as follows.

2.1.1. Statistical shape model

The process begins with the training step using M sample objects. Each shape S_b $(b = 1, 2, \ldots, M)$ of the training set is represented by N points corresponding to their spatial coordinates, $S_b = \{(x_{bi}, y_{bi}) | i = 1, 2, \ldots, N\}$. Shapes of the training set must be aligned to a reference shape. Several methods can be used for this purpose [21,38]. The mean shape $\bar{S}$ and the principal modes of variation are obtained by computing principal component analysis (PCA) to the set of aligned data. The statistical shape model is then calculated as

$$S = \bar{S} + Pf \tag{1}$$

where P is the matrix containing the set of eigenvectors corresponding to the highest eigenvalues (λ_l), f is a vector called shape parameter whose elements vary within the range $-3\sqrt{\lambda_l} \le f_l \le 3\sqrt{\lambda_l}$ [21,22].

2.1.2. Statistical texture model

The statistical texture model can essentially be obtained by following the same process carried out for the shape model. Here, the object texture is selected as the image patch enclosed by the shape points. Therefore, using the set of M texture samples described by $G_b = [g_{b1}, g_{b2}, \ldots, g_{bk}]$, where k is the size of the texture vector (number of pixels) obtained from the image patch and $g_{bj} (j = 1, 2, \ldots, k)$ is an intensity value, we align the training set to a reference texture. Warping methods are used for this purpose [39]. Similarly, a mean texture $\bar{G}$ and the principal modes of variation are calculated using PCA. The statistical texture model is written as

$$G = \bar{G} + Lr \tag{2}$$

Similarly, L is a matrix which contains the eigenvectors corresponding to the largest eigenvalues (σ_n) and r is the vector of texture parameter varying within the range $-3\sqrt{\sigma_n} \le r_n \le 3\sqrt{\sigma_n}$. By varying f in Eq. (1) and r in Eq. (2) we can generate new shapes and textures respectively.

2.1.3. *Combining statistical models: shape and texture*

A new robust and compact statistical model can be built by combining the shape and texture models. First, vectors b and r (shape and texture parameters) are concatenated in one vector d with the aim of using only one parameter to control both characteristics: shape and texture.

Therefore,

$$d = \begin{bmatrix} wf \\ r \end{bmatrix} = \begin{bmatrix} wP^{-1}(S_b - \bar{S}) \\ L^{-1}(G_b - \bar{G}) \end{bmatrix} \tag{3}$$

The term w is a weight matrix which normalizes the variation range between shape and texture parameters. This variable is necessary because shape parameters are measured in coordinates while texture parameters are measured in intensity values. A new stage of PCA is applied to vector d. As a result of the PCA stage, the final statistical model which combines shape and texture is found:

$$d = Qc \tag{4}$$

where Q is the set of eigenvectors selected according to the highest eigenvalues (ϑ) and c is the new vector of parameters used to control shape and texture simultaneously. New examples of texture and shape can be obtained by simply varying the vector c. Equations (1) and (2) are then rewritten as

$$S = \bar{S} + Pw^{-1}Q_S c \tag{5}$$

$$G = \bar{G} + LQ_G c \tag{6}$$

where Q_S and Q_G represent the combined set of eigenvectors of shape and texture respectively.

2.1.4. *Segmenting with AAM*

For segmentation of new images with AAM, it is required to find the parameter c that better fits the trained model to the new input image. This parameter guides the texture and shape models during the segmentation. The difference between the statistical texture model (I_{MI}) and the target image (I_{TI}) must be minimized. This is expressed as the vector δI.

$$\delta I = I_{TI} - I_{MI} \tag{7}$$

The original matching algorithm uses a linear regression method which was first developed in Ref. [21] and subsequently improved by Cootes and Taylor [40]. This method computes the difference δI to estimate the parameter c through each iteration. A regression matrix R has to be computed in the training process. This matrix codes the possible variations regarding the texture (intensity levels) and shape (rotation, translation and scaling) parameters. Therefore, new shape coordinates and texture map are calculated using Eqs. (5) and (6). This final information is taken as initialization for the next iteration. This procedure continues until the appearance model remains unchanged for a number of iterations.

2.2. *Proposed method*

Intensity changes of the input images may significantly reduce the segmentation performance of original AAM algorithms. It has been widely demonstrated that using intensity levels as raw texture data to build the active appearance model leads to inaccurate fitting during the AAM search [41–43]. Moreover, it is still more unpractical to code textures using original intensity values when working with fetal echocardiographic images. Here, the speckle pattern highly degrades the image quality, making almost impossible to identify features such as edges and homogeneous regions. The effect of using different texture patterns in AAM algorithms has been previously analyzed in Ref. [44] demonstrating that appearance model matching capabilities are improved when applying texture processors to the raw data. Nonetheless, robustness of texture matching applications is improved when texture codification is performed using other representation space through image transform tools [43,45–47]. The Gabor transform has been recently proposed for coding image textures in AAM [43,46]. Wavelet-based methods have also been used in combination with AAM for image segmentation [47].

Since AAM is a local method, the initialization process also becomes a critical problem for segmentation performance. The initial instance needs to be good enough in order to achieve an acceptable segmentation. Therefore, automatic algorithms based on AAM need efficient initialization methods.

In this work we propose a method which combines AAM and the steered HT for the left ventricle segmentation in fetal echocardiography. Coefficients of the steered HT are used to build the appearance models with the aim of improving the segmentation performance. The HT is relevant for image processing applications because it incorporates significant properties of the human visual system such as local directional analysis and Gaussian derivative models of early vision [28,33,43,48]. This transformation provides relevant details of images which are important for developing algorithms of medical image application [26,29,30]. Fig. 1 outlines the proposed scheme. It consists of three main stages: initialization, steered HT and multi-texture AAM segmentation. For the initialization process we have built a database which is used for matching purposes. Details for this database will be explained in this section as well.

2.2.1. *Database for initialization*

For initializing the algorithm, we built a database of image patches which includes the four cavities and descending aorta. These cardiac structures are illustrated in Fig. 2. These patches were selected from the set of training images. In order to cover the possible variations (orientations and sizes) present in the cardiac region, we have manually rotated and scaled the original image patches using several angles and scales respectively. Because we used image patches taken from the training set, we know the left ventricle position on each sample patch. The

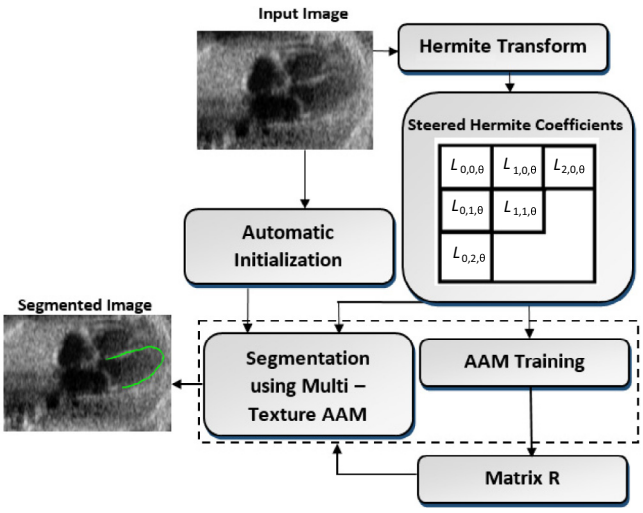

Fig. 1 – General scheme of the proposed multi-texture AAM method.

database was built using 15 images. We used 17 rotations within the range $[0, 2\pi]$ and two scales for each image. After rotating and scaling, the database finally consists of a total of 510 image patches. Image examples of the built database are shown in Fig. 3. It can be seen that images present different orientations and sizes regarding the heart region. By rotating each original image 17 times, i.e. each 21 degrees approximately, we can fill the space of possible variations with respect to the orientation. It is worth mentioning that this criterion is valid for images of our set of data. However, a database with more rotation angles can be built if needed. Fig. 3a shows the set of image patches obtained after performing 17 rotations of an original patch. The same criterion was applied to the number of scales used to build the database. In our case, it was enough to use two scales in order to cover the possible sizes for the left ventricle region in our set of data, considering phases from diastole to systole. Generally speaking, diastole is the phase where the left ventricle is more expanded and exhibits a bigger size with respect to systole phase. Fig. 3b shows image patches

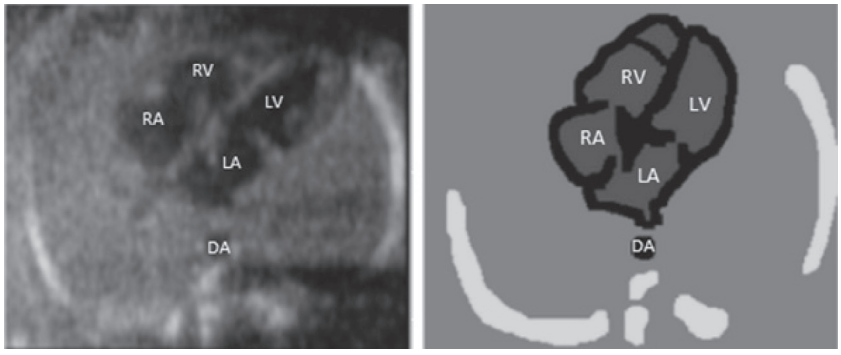

Fig. 2 – Fetal 4-chamber view. LA = left atrium; LV = left ventricle; RA = right atrium; RV = right ventricle; DA = descending aorta.

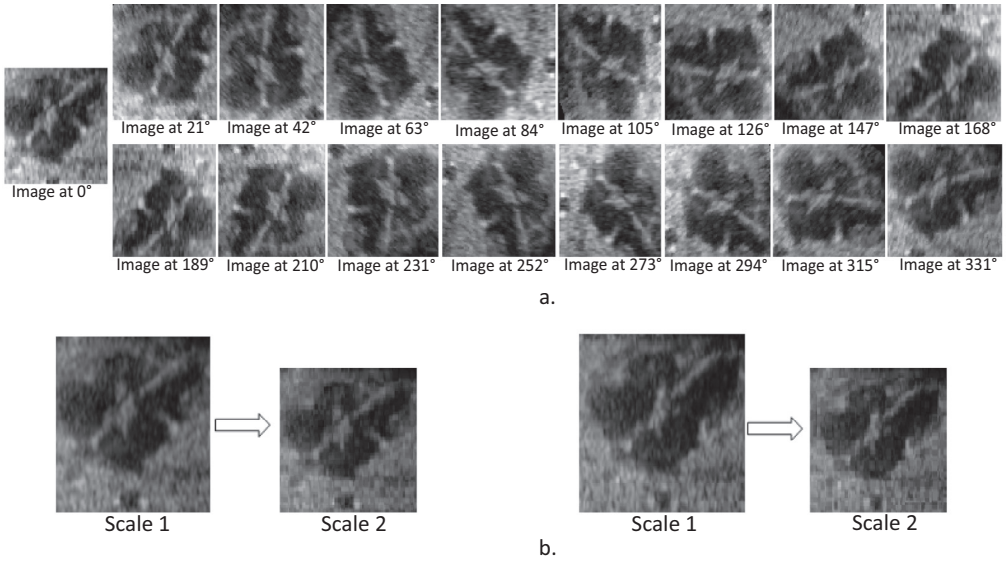

Fig. 3 – Image examples of the database used for initialization. (a) An image patch at seventeen different rotation angles. (b) Original and scaled patches at systole (left) and diastole (right) phases of the cardiac cycle.

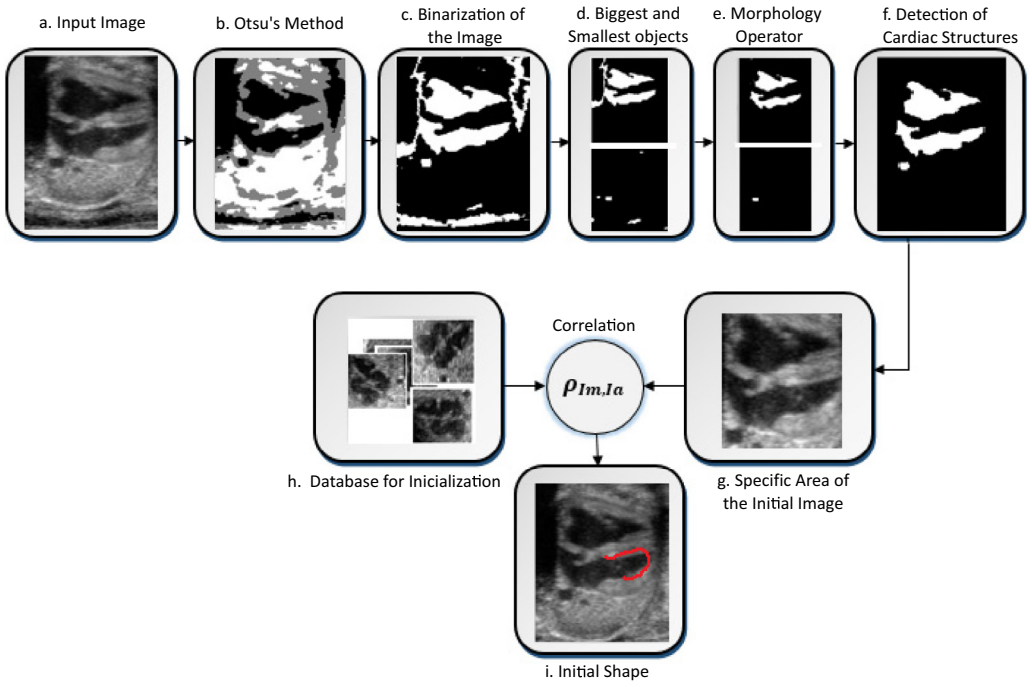

Fig. 4 – General diagram of the automatic initialization algorithm for left ventricle segmentation.

obtained after performing the scaling process. Examples are presented for both diastole and systole. Once the database has been stored it can be used to initialize the segmentation method for new examples. This is achieved using a matching process.

2.2.2. *Initialization*

We propose a novel initialization method which detects the left ventricle position inside the fetal cardiac ultrasound image. The heart cavities can exhibit different orientations inside the ultrasound image due to several reasons such as fetal and transducer positions during the acquisition process. It imposes a great challenge for the automatic initialization algorithm. The heart region size is also an important characteristic to take into account in the initialization process. Fig. 7 illustrates three examples with the typical variations depicted here.

The region of interest inside the heart includes the cavities and descending aorta (see Fig. 2) [49,50]. Even though in this work we are only interested in analyzing the left ventricle, we use the whole heart region in the initialization algorithm.

The initialization process is carried out through three stages. Fig. 4 presents a general diagram of the initialization algorithm. With a new input image to be segmented, the initialization algorithm follows these steps.

2.2.2.1. *ROI detection*. We first identify the region of interest in which the fetal heart is localized. For this purpose, a multilevel Otsu's thresholding method is used to divide the image into four different classes. Four regions can be identified inside the ultrasound image: background, cardiac structures such as four chambers and aorta, muscles and ribs (see Fig. 4b). Afterward, the second class is selected as the cardiac region (four chambers and aorta). The input image is then binarized according to this region. This step is shown in Fig. 4c. In order to find the cardiac structures, the biggest and smallest objects are selected from the binary image as shown in Fig. 4d (top and bottom respectively). We then apply morphology operators to remove some artifacts. The cardiac cavities finally correspond to objects with the biggest areas (Fig. 4e, top), and the aorta is the object with the smallest area which is closest to the cardiac cavities (see Fig. 4e, bottom). The final binary image is composed of the objects representing the cardiac cavities and aorta as shown in Fig. 4f.

2.2.2.2. *Correlation-based matching*. The ROI detection helps in identifying the region where cardiac structures are located. This region is then mapped into the original input image with the aim of selecting an image patch that includes the cardiac structures. This can be seen in Fig. 4g. Here, cross correlation is applied between this region and each patch of the previously stored database (see Fig. 4h). With this process we can identify the patch that better matches the selected region in the original image which contains the cardiac structures.

2.2.2.3. *Initial shape selection*. Finally, the database patch found in the last stage is used to pose the initial shape of the left ventricle. This can be achieved because coordinates of the left ventricle contour are known for each patch of the database. This final step is represented in Fig. 4i.

2.2.3. *Hermite transform (HT)*

The HT is a useful mathematical tool for image analysis applications. The decomposition process is locally obtained by first windowing the input image with a Gaussian function and then projecting it using orthogonal polynomials. In order to decompose the complete image, we have to shift the window to cover all possible positions. Here, the Hermite polynomials are employed to analyze the windowed information. They satisfy the orthogonal condition with respect to a Gaussian

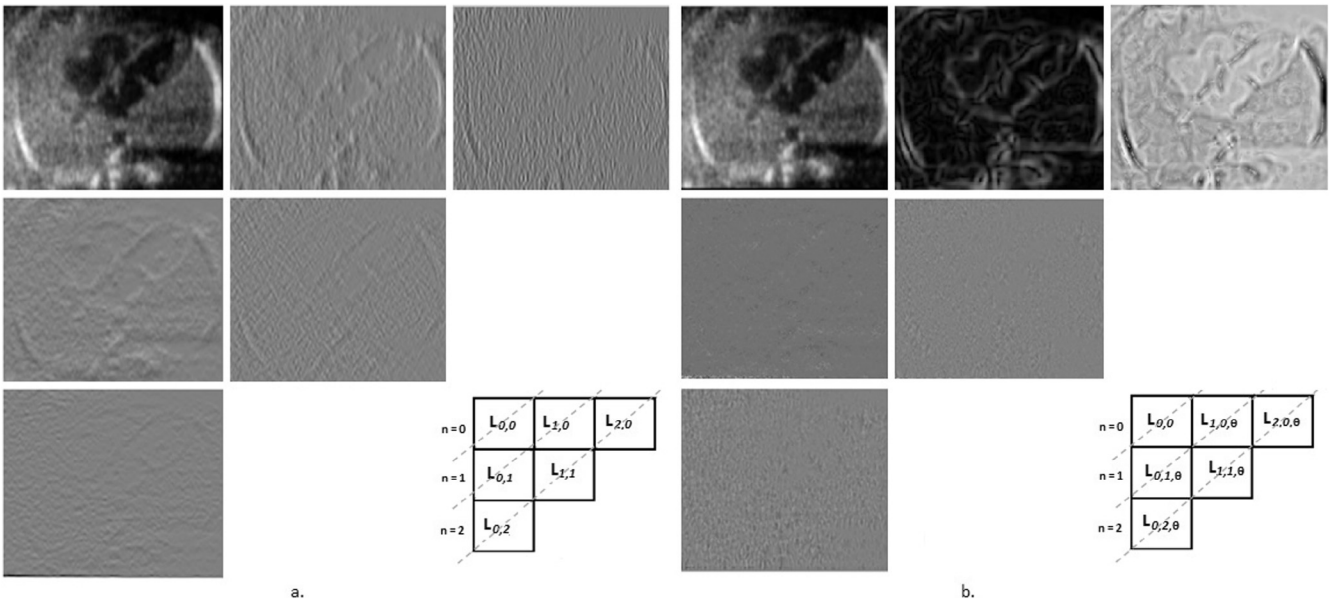

Fig. 5 – Hermite transform up to order n = 2: (a) Cartesian Hermite coefficients, (b) steered Hermite coefficients.

function: $\int\int_{-\infty}^{\infty} V^2(x,y)P_{m,n-m}(x,y)P_{l,k-l}(x,y)dxdy = \delta_{nk}\delta_{ml}$ [26,29,30], for $n,k = 0,1,\ldots,\infty$; $m = 0,1,\ldots,n$ and $l = 0,1,\ldots,k$; where $V(x,y) = \frac{1}{(\sigma\sqrt{\pi})} e^{\frac{-(x^2+y^2)}{2\sigma^2}}$, σ is the standard deviation of the Gaussian function, and $P_{m,n-m}(x,y) = \frac{1}{\sqrt{2^n(n-m)!m!}} H_m\left(\frac{x}{\sigma}\right) H_{n-m}\left(\frac{y}{\sigma}\right)$ are the normalized polynomials. Let $I(x,y)$ be an arbitrary function, the HT of I can be defined as

$$L_{m,n-m}(p,q) = \int\int_{-\infty}^{\infty} I(x,y)P_{m,n-m}(x-p,y-q)V^2(x-p,y-q)dxdy \quad (8)$$

where m and $n-m$ correspond to indices of the polynomials employed for the decomposition, $L_{m,n-m}$ corresponds to the cartesian Hermite coefficients, and n is the order of transformation. Each coefficient of the HT is simply obtained by convolving the input image with the set of filters described by: $D_{m,n-m}(x,y) = P_{m,n-m}(-x,-y)V^2(-x,-y)$, after subsampling at positions (p,q). According to the Hermite polynomial properties, the filters can be represented as Gaussian derivative operators:

$$D_{m,n-m}(x,y) = \frac{1}{\sqrt{2^n(n-m)!m!}} \left[\frac{d^m}{d\left(\frac{x}{\sigma}\right)^m} \frac{d^{n-m}}{d\left(\frac{y}{\sigma}\right)^{n-m}} V^2(x,y) \right] \quad (9)$$

where $V^2(x,y) = \frac{1}{(\sigma\sqrt{\pi})^2} e^{\frac{-(x^2+y^2)}{\sigma^2}}$.

Fig. 5a shows an example of the HT up to second order applied to an image of fetal echocardiography. Each coefficient of the HT is useful to find specific features of the input image such as edges, zero-crossings and texture.

2.2.4. *Steered Hermite transform*

A main characteristic of the HT is that local directional analysis can be performed [27,28,31–33] by steering the cartesian Hermite coefficients. The process is made through a linear combination of the cartesian coefficients [31,32].

From a mathematical point of view, coefficients are then separated in spatial and polar domains and their Fourier transform can be now written in polar coordinates. With $\omega_x = \omega \cos\theta$ and $\omega_y = \omega \sin\theta$ this can be expressed by:

$$d_m(\omega_x)d_{n-m}(\omega_y) = q_{m,n-m}(\theta)\cdot d_n(\omega) \quad (10)$$

where $d_n(\omega)$ represents the Fourier transform of each filter:

$$d_n(\omega) = \frac{1}{\sqrt{2^n n!}} (-j\omega\sigma)^n e^{-(\omega\sigma)^2/4} \quad (11)$$

Filter orientation is given by:

$$q_{m,n-m}(\theta) = \sqrt{\binom{n}{m}} \cos^m\theta \cdot \sin^{n-m}\theta \quad (12)$$

Considering the orientation frequency functions, this property of the Hermite filters can be defined as

$$q_{m,n-m}(\theta-\theta_0) = \sum_{i=0}^{n} c_{m,i}^{(n)}(\theta_0) q_{n-i,i}(\theta) \quad (13)$$

where $c_{m,i}^{(n)}(\theta_0)$ are the steering coefficients. Finally, the steered Hermite coefficients are obtained by:

$$L_{m,n-m,\theta} = \sum_{i=0}^{n} q_{i,n-i} L_{i,n-i} \quad (14)$$

where $L_{m,n-m,\theta}$ are the steered coefficients. Fig. 5b shows the steered HT calculated for coefficients previously obtained in Fig. 5a. A great advantage of the steered HT is that most of the energy is concentrated in a few coefficients (first line of

coefficients in scheme of Fig. 5b). More details about the HT and its steering property can be reviewed in Refs. [26–33].

2.2.5. *Multi-texture AAM*

From an image processing point of view, it is well known that the speckle pattern is one of the main problems to handle when analyzing ultrasound images. Generally speaking, images with speckle are difficult to process because edges are not visible and seem to be unconnected. Moreover, regions of the objects of interest are not homogeneous. This problem has encouraged researchers to design denoising algorithms to improve the detection performance in ultrasound images. There is a tendency to take advantage of the speckle pattern in order to extract texture information implicit in the speckle pattern, instead of using denoising algorithms [51,52] . The reason is that there is valuable information regarding the object of interest which can be modified if a filtering process is previously applied. This idea is followed in this work and we propose to use the steered HT as mechanism to code texture information without using a denoising stage. Here, local spatial relationships between neighboring pixels are efficiently obtained by applying this polynomial transformation.

The steered Hermite coefficients up to second order $(L_{0,0}, L_{1,0,\theta}, L_{2,0,\theta})$ are used to build the proposed multi-texture AAM. For this purpose, an independent AAM is created for each steered coefficient. Our goal is to combine these models in order to obtain an efficient segmentation. Three different texture patterns are processed with these coefficients: intensity, edges and zero-crossings. With this method we aim at providing a robust scheme which is able to address the segmentation by analyzing three types of image features. Two main steps are followed in this process.

The first step consists of building an AAM for each steered coefficient in order to code its statistical properties. It implies to compute the steered HT using images of the training set and then build an AAM for each selected coefficient.

The second step corresponds to the active search in which the stored statistical models are used for segmentation of new images. We assume that the steered Hermite transform up to order $n = 2$ has been previously applied to the input image. Moreover, the initialization stage has also been performed and an initial shape has been obtained. Then, using the initial shape position, the input texture pattern is obtained. In this step, each steered Hermite coefficient and its corresponding trained model must be processed. Here, we will assume that $j0$ indicates a particular steered coefficient, with $j = 0,1,2$. The difference (δI_{j0}) between the input texture pattern and statistical texture model obtained from training must be calculated using Eq. (7). The vector of parameters co_{j0} which controls the shape and texture variations of the appearance model is subsequently computed. Then, the optimum co_{j0} is updated as follows:

$$co_{j0}^{t} = co_{j0}^{t-1} - R_{j0}\delta I_{j0} \tag{15}$$

where R_{j0} is the regression matrix obtained during the training stage and t indicates the current iteration. The algorithm active search is an iterative process which needs an initial co_{j0}^{0}. Normally, it is set to zero. As mentioned, by using co_{j0}^{t} we can update the statistical shape and texture models. For the latter, Eq. (6) is employed. It means that the statistical texture model is updated for each steered Hermite coefficient independently. Since we are finally interested in obtaining only the contour of the segmentation, we propose to compute a general statistical shape model by performing a weighted combination using all the shape models obtained for the steered coefficients. Equation (5) is therefore modified as

$$S_t = \sum_{j=0}^{2} a_j\left(\bar{S}_{j0} + P_{j0}w_{j0}^{-1}Q_{j0}co_{j0}^{t}\right) \tag{16}$$

where a_j corresponds to weights assigned to each shape model, normalized to $\sum_{j=0}^{2} a_j = 1$. Since the segmentation objective is to find better positions for the initial shape points, we only use a combination of the shape models. However, the input texture patterns and statistical texture models guide the appearance models deformation. The algorithm is iterative and the result in Eq. (16) is used as initialization for the next iteration.

Fig. 6 shows examples of two modes of variation of the statistical texture models used in this work. They were obtained for the steered Hermite coefficients selected to construct the multi-texture AAM.

3. Experiments and results

Results of the implemented method were evaluated using real ultrasound images of the fetal heart. The left ventricle acquired at the original axial view was used for analysis. We compared the proposed method results with other related and common approaches found in the literature. Quantitative and qualitative performances are presented in this section.

3.1. *Materials*

For evaluation of the proposed method we used a total of 10 study cases, each one corresponding to a different patient. They were acquired from normal fetuses without cardiomyopathies. In total, we have 143 real ultrasound images showing the fetal heart at several phases of the cardiac cycle from diastole to systole. All studies were provided and collected by Instituto Nacional de Perinatología, México. Ultrasound studies were acquired with a Volunson E8 system of General Electric. All images were manually segmented by the physician. Image size varies from 190×230 to 360×280, quantized to 8 bits per pixel. All test images present variations regarding heart position, size and contrast.

3.2. *Performance evaluation*

We used a database of 98 annotated images corresponding to 5 patients for training the multi-texture AAM. The left ventricle contour was subsampled using 50 landmarks. A total of 45 images corresponding to the rest of patients were used for validation. Images at different phases of the cardiac cycle were evaluated.

3.2.1. *Initialization algorithm*

Initialization is a critical stage for active appearance models. Since AAM is a local method, the initial contour needs to be

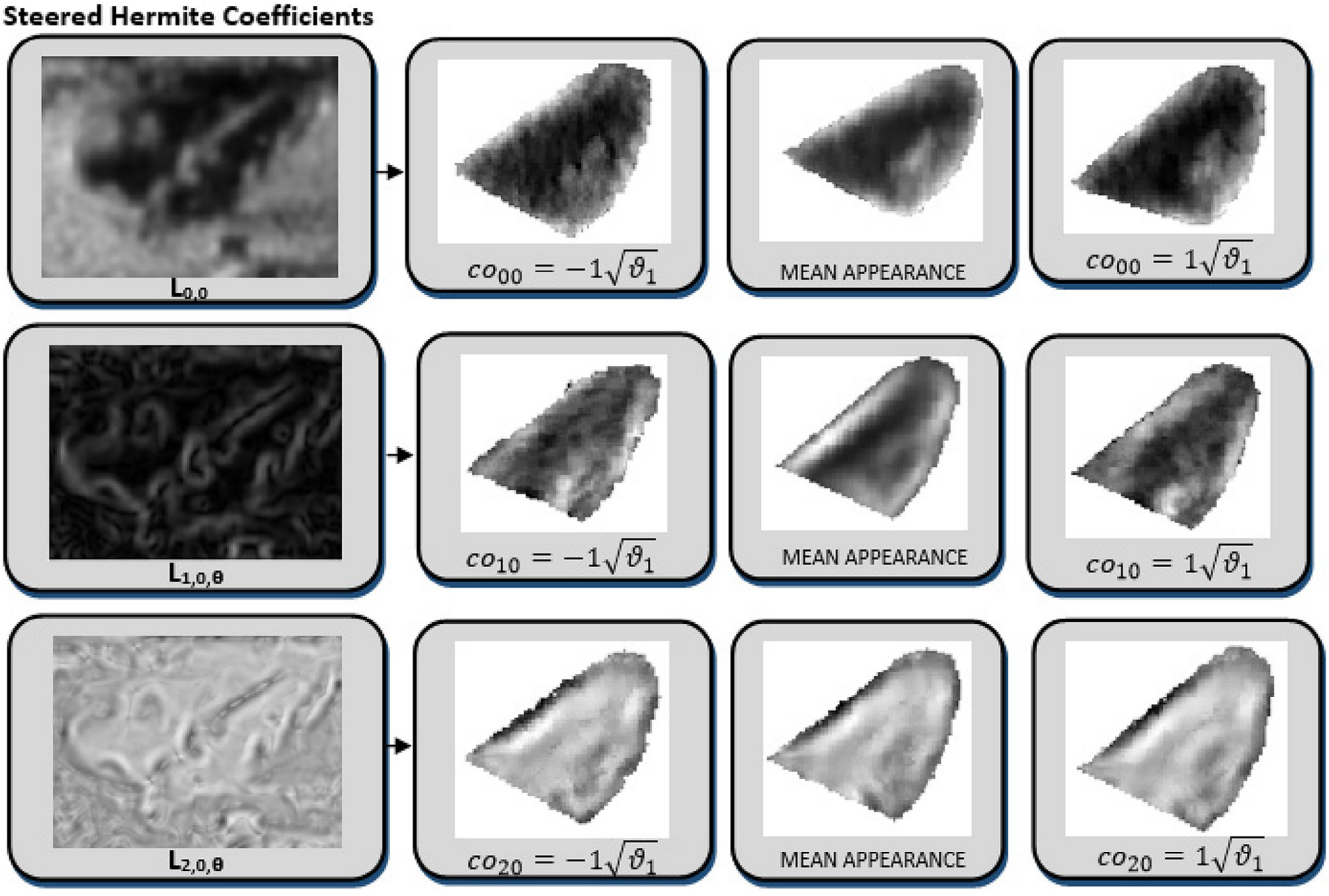

Fig. 6 – Two modes of variation of the statistical models using texture maps given by coefficients $L_{0,0}$, $L_{1,0,\theta}$ and $L_{2,0,\theta}$ of the steered HT. ϑ corresponds to the first eigenvalue obtained for each appearance model (see Section 2.1.3).

near the left ventricle. Fig. 7 illustrates initialization results using three images of our dataset.

As mentioned, the cardiac cavities may present different orientations and scales in fetal cardiac ultrasound images. It can be seen in Fig. 7 how our proposed initialization algorithm can handle these types of variations.

Table 1 presents quantitative evaluation of the initialization algorithm. The Euclidean distance (reported in pixels), Dice coefficient and error of the estimated orientation were computed. These metrics were calculated by comparing the initial pose with the ground truth. The orientation was obtained with respect to the major axis of the left ventricle cavity.

We prepared an experiment to evaluate how the initial pose changes with respect to the number of database image patches. Here, we selected a test image which was subsequently compared with databases containing different numbers of patch images. To build each database, we selected 15 image patches which were posteriorly scaled and rotated. Here, we used two cases: (1) in the first case (one scale), 15 original patches were rotated without scaling; (2) in the second case (two scales), 15

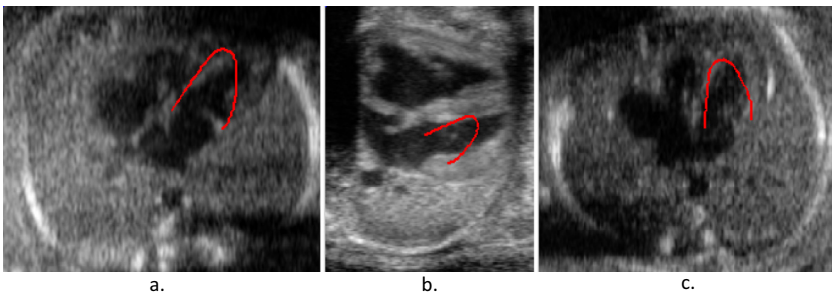

Fig. 7 – Results of the initialization process (red contour) using three different test images. Differences regarding the position and scale of the left ventricle and the rest of cardiac cavities are seen in these examples. (For interpretation of the references to color in this figure legend, the reader is referred to the web version of this article.)

Table 1 – Quantitative evaluation of the initialization algorithm.

Initialization	Patient 1	Patient 2	Patient 3	Patient 4	Patient 5
Orientation error	10.30 ± 5.36	24.59 ± 7.51	16.46 ± 6.90	7.40 ± 4.18	5.32 ± 4.56
Distance	9.16 ± 3.26	20.40 ± 4.54	8.62 ± 2.61	7.59 ± 3.67	3.78 ± 1.32
Dice	0.70 ± 0.07	0.65 ± 0.08	0.73 ± 0.03	0.75 ± 0.02	0.79 ± 0.03

patches were scaled one time and then rotated. Therefore, the exact number of image patches of the database for each proof depends on the number of rotations used. Fig. 8 shows the results for this experiment. The blue curve was obtained using a database built for one scale and the red curve was obtained using image patches with two scales. The horizontal axis corresponds to the number of rotations used to build the database. The vertical axis is the minimal error obtained in the matching process between the test image and each database. An interesting finding in these curves is that the initial pose error does not change if we use a database with more than 17 rotations for each case approximately. The reason is that after a specific number of rotations, the best match for the test image has been included in the database and adding more images does not produce significant changes. Naturally, this behavior is valid for our set of test images and it can be different with other set of data.

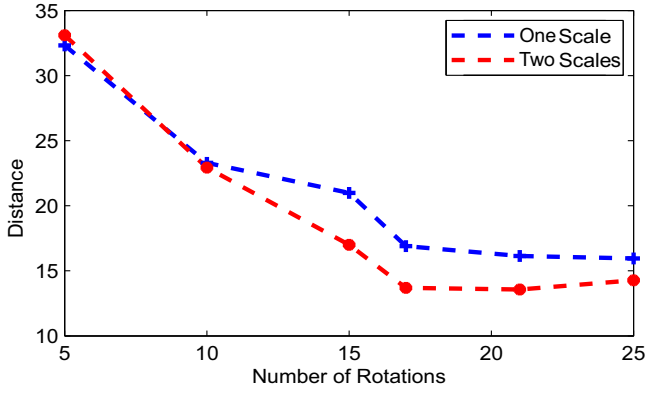

Fig. 8 – Results of the matching process when using databases with different quantity of image patches. This value is controlled by building databases using different number of rotations and scales. The blue curve was obtained using patches with one scale and the red curve with two scales. (For interpretation of the references to color in this figure legend, the reader is referred to the web version of this article.)

3.2.2. *Multi-texture AAM algorithm*

The algorithm was set up to run until 30 iterations. Experimentally, we found that the best weights for the multi-texture AAM are $w_i = \frac{1}{3}$ with i = 1, 2, 3.

Fig. 9 shows an image of our dataset with segmentation results for several iterations of the algorithm. Fig. 9a corresponds to the initial shape resulted from the initialization process. Fig. 9b, 9c, 9d, 9e and 9f are the resulting shapes after 2, 7, 10, 20 and 30 iterations, respectively. For this example the algorithm converged after 11 iterations. Fig. 9f shows the initial shape (red contour) and final segmentation (green contour). The initial shape is closed to the left ventricle which allows a faster convergence of the algorithm. It can be seen that the initial shape is slightly rotated with respect to the major axis of the left ventricle. Our trained multi-texture AAM corrected the initial shape position to reach an efficient segmentation. Although

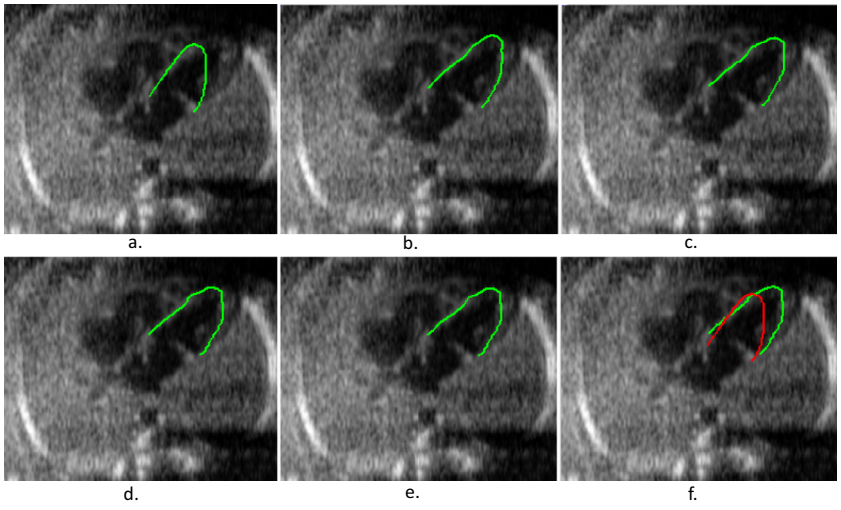

Fig. 9 – Results of the left ventricle segmentation obtained for several iterations: (a) initial shape, (b) iteration 2, (c) iteration 7, (d) iteration 10, (e) iteration 20, (f) iteration 30 (The green line is the final result and the red line is the initial shape). (For interpretation of the references to color in this figure legend, the reader is referred to the web version of this article.)

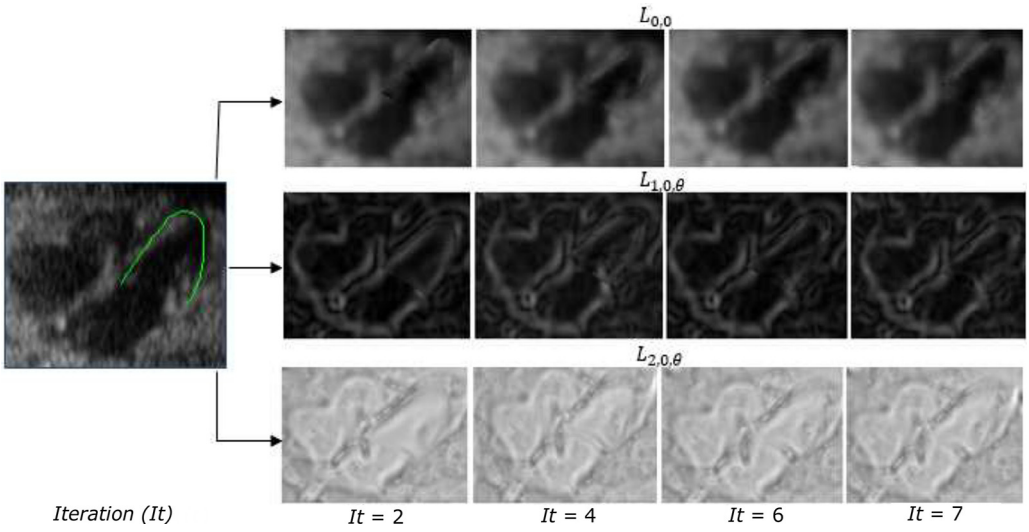

Fig. 10 – Deformation of the appearance model built for each steered Hermite coefficient for several iterations.

the initial shape was misaligned, it was very closed to the left ventricle which helped to achieve a good result.

Active appearance models deform not only the shape but also the object texture. In our multi-texture AAM we have used three coefficients of the steered HT to build the statistical texture models. Fig. 10 depicts the texture deformation using a test image of our dataset. It was taken at the beginning of the diastole. Coefficients $L_{0,0}, L_{1,0,\theta}, L_{2,0,\theta}$ are shown. Texture deformation is illustrated for several iterations. The first image which contains the green contour is the original image with the initial shape. We can see how the initial texture changes until reaching a stable state in iteration 7. The sequence of warping and adjusting of the patch texture to achieve the best match between the texture model and target image is visualized. Images in the last column (Iteration 7) show the final patch texture achieved with the multi-texture AAM.

For quantitative analysis we used two different metrics. First, we calculated the point-to-curve distance between the manual and automatic segmentation. Here, we compared with other classic segmentation methods. Results were obtained for five clinical cases corresponding to 45 images acquired for the complete cardiac cycle. In Table 2, we present the obtained results of the segmentation methods. Each clinical case was taken from a different patient and corresponds to a complete sequence of the heart cycle. Each sequence is also composed of a different number of images. We have averaged results for all images of the sequences and they are presented in pixel values. As seen, our proposed framework outperforms the rest of segmentation methods in all cases.

On the other hand, the algorithm performance was also evaluated using the Dice similarity coefficient. This second measure is used to calculate the degree of similarity between the manual annotation and segmentation obtained with the proposed algorithm. Both segmentations are used to compute the overlapping region between them. Fig. 11 shows the results of the Dice similarity coefficient obtained for the five patients of our dataset. The coefficient was averaged for all images of each sequence. Similarly, we compared results achieved with our method against other segmentation approaches. Results are presented using a color bar diagram. In all cases, the developed method (red bar) in this work exhibits the best performance. Considering individual results using all test images, the best result obtained with our method was 0.963 which corresponds to an image at the beginning of the diastole phase. The worst result was 0.7887 corresponding to an image at the end of the systole. The obtained contours for these two cases can be seen in Fig. 12.

Fig. 13 shows graphical segmentation results using several methods and the proposed approach. The red contour is the expert delineation and the green contour is the segmentation obtained with each method. Visually, our method presents the best performance.

We also present a test of convergence for our algorithm using an image example. This test is compared with three of the other segmentation methods (see Fig. 14). The error between the manual and automatic segmentation was computed for 30 iterations. It can be noted that the Snake method presents the fastest convergence because it only evaluates profiles for each

Table 2 – Average point-to-curve distance obtained for 5 patients, the proposed method is compared with others found in the literature. The expert segmentation was taken as the ground truth. Distance values are expressed in mean ± STD.

Patients	Snake	ASM	Classic AAM	AAM with LBP	Multi-texture AAM
Patient 1 (9 images)	5.40 ± 4.58	5.27 ± 3.62	3.35 ± 1.86	5.16 ± 2.47	2.16 ± 1.15
Patient 2 (11 images)	4.76 ± 4.05	4.61 ± 4.23	3.42 ± 1.85	4.11 ± 2.82	2.21 ± 0.60
Patient 3 (7 images)	4.13 ± 3.80	4.16 ± 2.09	3.03 ± 1.08	4.15 ± 3.60	1.94 ± 1.21
Patient 4 (6 images)	6.37 ± 4.26	4.76 ± 4.22	3.55 ± 1.03	5.51 ± 2.90	1.87 ± 0.95
Patient 5 (12 images)	6.36 ± 5.98	5.02 ± 4.11	2.21 ± 1.90	6.06 ± 4.35	1.92 ± 0.92

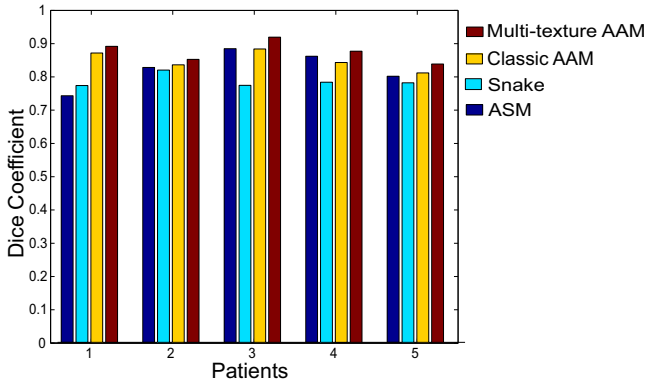

Fig. 11 – Dice coefficient obtained with the proposed approach and three methods used for comparison purposes.

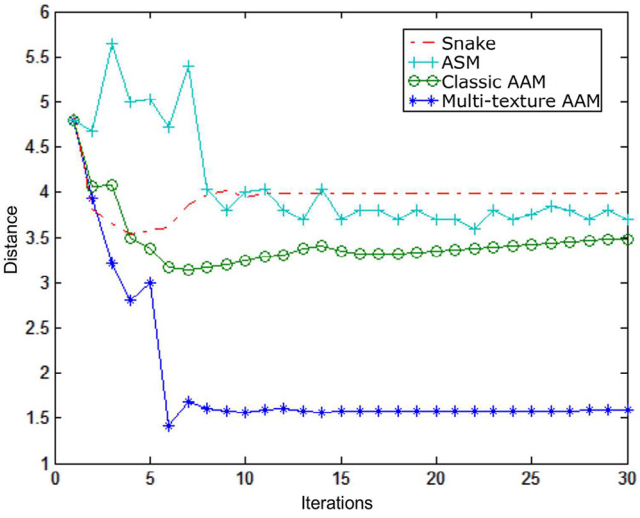

Fig. 14 – Evolution of the point-to-curve distance. Four methods are evaluated: Snake, ASM, AAM and the proposed multi-texture AAM.

point to find the minimum energy of its functional. Since it is based on gradient functions, its performance is poor with ultrasound images. The ASM method also uses gray level and gradient profiles but it is limited to a range of deformation. The performance of ASM is better than Snake but the stability is lost due to the image noise. The multi-texture AAM converges slower than Snake but faster and more stable than AAM and ASM. Our method also presents the best final result. The texture coefficients of the steered HT improve the segmentation performance because several features of the image patches are coded. This behavior was similar for the rest of images.

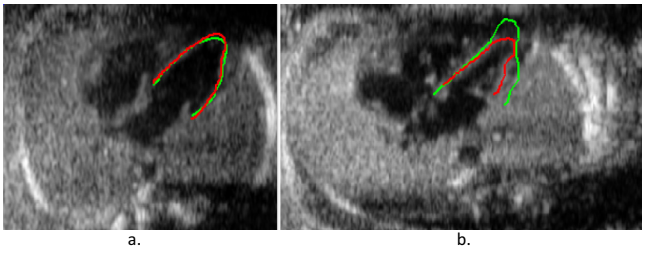

Fig. 12 – Best and worst Dice coefficients obtained for individual images of our dataset: the green contour is the automatic segmentation and the red contour is the manual annotation. (a) Best result (image at the end-diastolic phase), (b) worst result (image at the end-systolic phase). (For interpretation of the references to color in this figure legend, the reader is referred to the web version of this article.)

It is well known that during the heart cycle, from diastole to systole, the size and shape of the left ventricle may change significantly. In the following experiment, we evaluated the performance of the proposed method for all phases of the cardiac cycle. For this purpose, we used two sequences of our dataset and computed the segmentation error for each image of the sequence. A total of 19 images were used for each sequence. Fig. 15 illustrates these results. It can be seen that the best performances were obtained for the diastole and beginning of the systole phase. The worst performance was achieved during the end of the systole phase where the left ventricle is smaller and its shape is more irregular. This leads to failure of the adaption

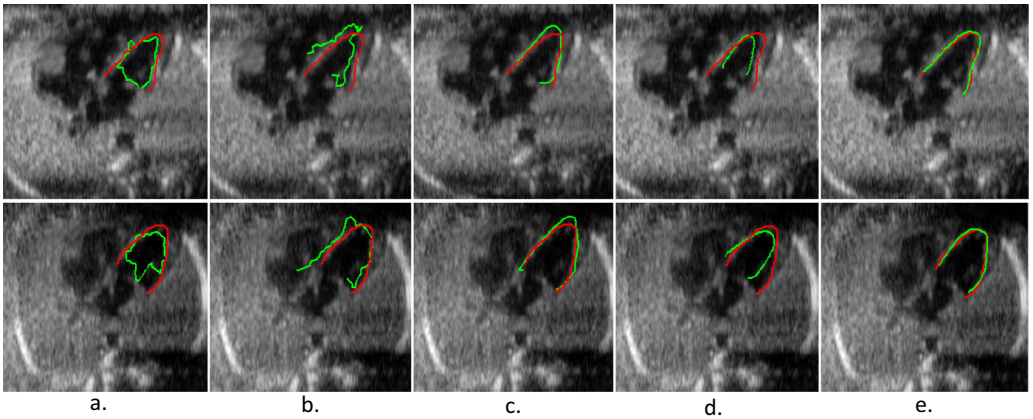

Fig. 13 – Results of the segmentation using two test images and five methods employed for comparison purposes: (a) Snake, (b) ASM, (c) AAM, (d) AAM with LBP, (e) proposed multi-texture AAM.

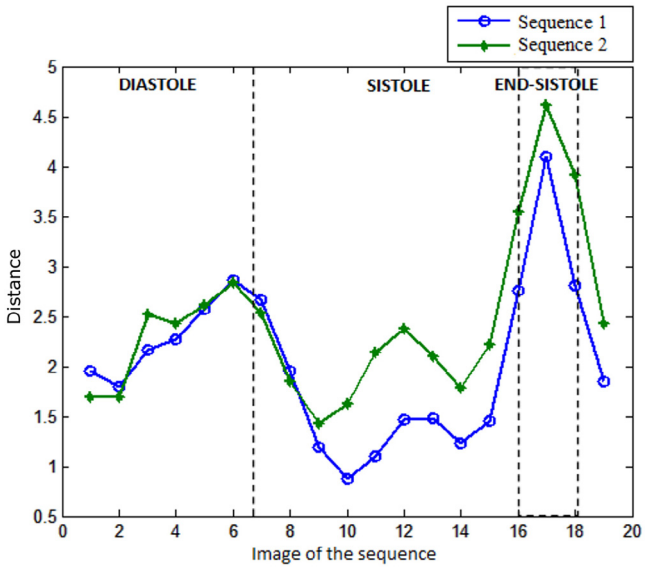

Fig. 15 – Point-to-curve distance obtained for two test sequences. The error is evaluated for the entire cardiac cycle.

process of the multi-texture AAM. An interesting finding in this experiment is that the behavior was very similar for both sequences.

One of the critical issues of the proposed multi-texture AAM is the weight values choice in Eq. (16). Since our method is the weighted combination of several appearance models, we must decide which texture coefficients are more relevant for a particular example. Although there is not a defined rule to assign the weight values, we performed an experiment to determine the optimal weights for all images of our dataset. We tested the algorithm for 4 cases: $a1 > (a2, a3)$, $a2 > (a1, a3)$, $a3 > (a1, a2)$ and $a1 = a2 = a3$. We present the averaged results for all cases using the point-to-curve distance and the Dice coefficient in Table 3. It can be seen that the best performance was achieved when all weights have the same value. Similarly, we show the obtained contours for a test image in Fig. 16. Several weights were used and the best contour was obtained for the case when $a1 = a2 = a3$ which corresponds to the red contour.

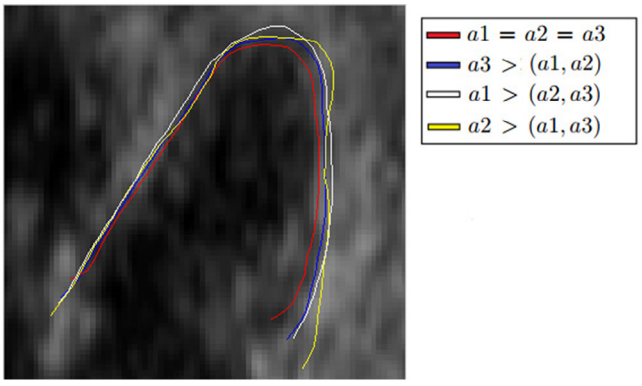

Fig. 16 – Contours of the left ventricle segmentation applying four different criteria for the weight parameters of the multi-texture AAM.

Table 3 – Effect of varying the weight parameters in the multi-texture AAM. Point-to-curve distance and Dice coefficient are

Weight parameters	Distance Mean ± STD	Dice
$a1 > a2$ and $a1 > a3$	2.83 ± 2.12	0.83
$a2 > a1$ and $a2 > a3$	3.01 ± 1.96	0.80
$a3 > a1$ and $a3 > a2$	2.10 ± 1.57	0.84
$a1 = a2 = a3$	1.72 ± 1.16	0.85

4. Discussion and conclusions

As seen in Fig. 7, fetal cardiac ultrasound images can exhibit different orientations and shape variations of the cardiac cavities. Commonly, it is difficult to find the boundaries that separate the left ventricle from the atrium. This specific case depends on the gestation period, skills to acquire the echocardiographic images and ultrasound system. Taking into account the mentioned problems, it is very challenging to automatically find the position and orientation of the left ventricle inside the ultrasound image using an automatic algorithm.

The initialization method proposed in this work overcomes these problems. It consists of a simple but effective method capable to generate the initial contour of the left ventricle cavity. Based on an object detection process, the region corresponding to cardiac structures is first identified and then a correlation process is used to find the initial pose. Fig. 7 and Table 1 illustrate the effectiveness of the algorithm. With the initialization achieved, the proposed algorithm is efficiently adjusted to reach the desired segmentation. The initialization method only requires to store a database with sample patches describing the possible variations found in fetal echocardiographic images. Although there are other robust methods for matching and object detection in the literature, they normally require robust training processes and huge databases of image samples. Moreover, the matching process using correlation between an input image and a database has been also successfully used in other applications [53,54].

We have presented quantitative comparisons between the proposed method and other approaches described in the literature. These methods are classic AAM, Snake, ASM and AAM with LBP. Quantitative results were shown in Table 2 and Fig. 11. Qualitative results can be seen in Fig. 13 for two test images. In all cases, the proposed multi-texture AAM outperforms results of the other methods.

ASM and Snake present the poorest results because they are based on boundary detection functions. It is well known that ultrasound images lack well-defined edges. Classic AAM presents better results than ASM and Snake because it is guided by the texture patch of the object. However, it uses the texture of the original image which is not adequate when working with ultrasound images. AAM with LBP also presents a lower performance compared to the proposed approach. Methods based on LPB use differences of intensities to code image texture. This is not suitable for ultrasound images due to the speckle pattern either. An interesting finding here is that using AAM with LBP was even less effective than classic AAM. In our multi-texture

map of the original images, we used coefficients of the steered HT. We combined the texture models in one weighted scheme in order to include more descriptive textures of the original image. With this simple and effective scheme, we improved the segmentation results of the standard AAM.

One of the main issues when segmenting fetal cardiac ultrasound sequences is the shape variation during the cardiac cycle. Results in Fig. 15 demonstrate that the worst performance occurs when the left ventricle is at the phase of most contraction, this is, at end-systole. The left ventricle is more irregular and cavity homogeneous regions are not well-defined, making this region more difficult to segment. Fig. 12 shows two image examples which depict how the left ventricle significantly changes from the end-diastolic to end-systolic phase.

The implemented framework can be a useful tool for evaluating the left ventricle in fetal echocardiographic sequences. Our results are better than other reported methods in the literature [25,34–37]. We obtained an average Dice coefficient of 0.8631 and average point-to-curve distance of 2.027. The segmentation results were very encouraging in images with large variations in the left ventricle.

Conflict of interest

None declared.

Acknowledgments

This work has been sponsored by the following grants: UNAM PAPIIT IG100814, SECITI 110/2015. Lorena Vargas-Quintero thanks CONACYT—255035 for the financial support, as well as Colciencias. The authors thank the Instituto Nacional de Perinatología, México, for all the support in this work.

REFERENCES

[1] J. Bushberg, The Essential Physics of Medical Imaging, Lippincott Williams & Wilkins, Philadelphia, 2002.
[2] F.-D. Lebit, R. Vladareanu, The role of 4D ultrasound in the assessment of fetal behaviour, Maedica (Buchar) 6 (2) (2011) 120–127.
[3] O. Eskandar, S. Eckford, T. Watkinson, Safety of diagnostic imaging in pregnancy. Part 2: magnetic resonance imaging, ultrasound scanning and Doppler assessment, Obstet. Gynecol. 12 (3) (2010) 171–177.
[4] D.L. Miller, Safety assurance in obstetrical ultrasound, Semin. Ultrasound CT MR 29 (2008) 156–164.
[5] J. Simpson, Echocardiographic evaluation of cardiac function in the fetus, Prenat. Diagn. 24 (13) (2004) 1081–1091.
[6] J.S. Abramowicz, Benefits and risks of ultrasound in pregnancy, Semin. Perinatol. 37 (2013) 295–300.
[7] J. Rychik, N. Ayres, B. Cuneo, N. Gotteiner, L. Hornberger, P.J. Spevak, et al., American society of echocardiography guidelines and standards for performance of the fetal echocardiogram, J. Am. Soc. Echocardiogr. 17 (7) (2004) 803–810.
[8] J.I. Hoffman, S. Kaplan, The incidence of congenital heart disease, J. Am. Coll. Cardiol. 39 (12) (2002) 1890–1900.
[9] F. Molina, C. Faro, A. Sotiriadis, T. Dagklis, K. Nicolaides, Heart stroke volume and cardiac output by four-dimensional ultrasound in normal fetuses, Ultrasound Obstet. Gynecol. 32 (2) (2008) 181–187.
[10] A.K. Younoszai, D.E. Saudek, S.P. Emery, J.D. Thomas, Evaluation of myocardial mechanics in the fetus by velocity vector imaging, J. Am. Soc. Echocardiogr. 21 (5) (2008) 470–474.
[11] R. Wagner, S. Smith, J. Sandrik, H. Lopez, Statistics of speckle in ultrasound B-scans, IEEE Trans. Sonics Ultrason. 30 (3) (1983) 156–163.
[12] Y. Guo, Y. Wang, D. Kong, X. Shu, Automatic segmentation of cardiac tumor in echocardiogram based on sparse representation and modified ACM, Instructions for Oral/Poster Presentations, 2012, 13.
[13] J.A. Noble, D. Boukerroui, Ultrasound image segmentation: a survey, IEEE Trans. Med. Imaging 25 (8) (2006) 987–1010.
[14] M. Marsousi, A. Eftekhari, A. Kocharian, J. Alirezaie, Endocardial boundary extraction in left ventricular echocardiographic images using fast and adaptive B-spline snake algorithm, Int. J. Comput. Assist. Radiol. Surg. 5 (5) (2010) 501–513.
[15] N. Paragios, M.-P. Jolly, M. Taron, R. Ramaraj, Active shape models and segmentation of the left ventricle in echocardiography, in: Scale Space and PDE Methods in Computer Vision, Springer, Berlin Heidelberg, 2005, pp. 131–142.
[16] G. Hamarneh, T. Gustavsson, Combining snakes and active shape models for segmenting the human left ventricle in echocardiographic images, in: Computers in Cardiology 2000, IEEE, Piscataway, NJ, 2000, pp. 115–118.
[17] T. Cootes, A. Hill, C. Taylor, J. Haslam, Information processing in medical imaging use of active shape models for locating structures in medical images, Image Vis. Comput. 12 (6) (1994) 355–365.
[18] J.G. Bosch, S.C. Mitchell, B.P. Lelieveldt, F. Nijland, O. Kamp, M. Sonka, et al., Automatic segmentation of echocardiographic sequences by active appearance motion models, IEEE Trans. Med. Imaging 21 (11) (2002) 1374–1383.
[19] N. Lin, W. Yu, J.S. Duncan, Combinative multi-scale level set framework for echocardiographic image segmentation, Med. Image Anal. 7 (4) (2003) 529–537 Medical Image Computing and Computer Assisted Intervention.
[20] M. Hansson, S.S. Brandt, J. Lindström, P. Gudmundsson, A. Jujić, A. Malmgren, et al., Segmentation of B-mode cardiac ultrasound data by Bayesian probability maps, Med. Image Anal. 18 (7) (2014) 1184–1199.
[21] T.F. Cootes, G.J. Edwards, C.J. Taylor, Active appearance models, IEEE Trans. Pattern Anal. Mach. Intell. (6) (2001) 681–685.
[22] T.F. Cootes, C. Beeston, G.J. Edwards, C.J. Taylor, A unified framework for atlas matching using active appearance models, in: Information Processing in Medical Imaging, Springer, Berlin Heidelberg, 1999, pp. 322–333.
[23] X. Chen, J.K. Udupa, U. Bagci, Y. Zhuge, J. Yao, Medical image segmentation by combining graph cuts and oriented active appearance models, IEEE Trans. Image Process. 21 (4) (2012) 2035–2046.
[24] S. Nandagopalan, B. Adiga, C. Dhanalakshmi, N. Deepak, Automatic segmentation and ventricular border detection of 2D echocardiographic images combining k-means clustering and active contour model, in: 2010 Second International Conference on Computer and Network Technology (ICCNT), IEEE, Singapore, 2010, pp. 447–451.

[25] Y. Guo, Y. Wang, S. Nie, J. Yu, P. Chen, Automatic segmentation of a fetal echocardiogram using modified active appearance models and sparse representation, IEEE Trans. Biomed. Eng. 61 (4) (2014) 1121–1133.
[26] J.-B. Martens, The Hermite transform-applications, IEEE Trans. Acoust. 38 (9) (1990) 1607–1618.
[27] J.-B. Martens, The Hermite transform-theory, IEEE Trans. Acoust. 38 (9) (1990) 1595–1606.
[28] A. Estudillo-Romero, B. Escalante-Ramirez, Rotation-invariant texture features from the steered Hermite transform, Pattern Recognit. Lett. 32 (16) (2011) 2150–2162.
[29] B. Escalante-Ramírez, E. Moya-Albor, L. Barba-J, F. Arambula Cosio, E. Vallejo, Motion estimation and segmentation in CT cardiac images using the Hermite transform and active shape models, Proc. SPIE 8856 (2013) 88561E–88561E-15.
[30] B. Escalante-Ramrez, The Hermite transform as an efficient model for local image analysis: an application to medical image fusion, Comput. Electr. Engi. 34 (2) (2008) 99–110.
[31] W.T. Freeman, E.H. Adelson, The design and use of steerable filters, IEEE Trans. Pattern Anal. Mach. Intell. 9 (1991) 891–906.
[32] J.L. Silván-Cárdenas, B. Escalante-Ramírez, The multiscale Hermite transform for local orientation analysis, IEEE Trans. Image Process. 15 (5) (2006) 1236–1253.
[33] E. Moya-Albor, B. Escalante-Ramrez, E. Vallejo, Optical flow estimation in cardiac ct images using the steered Hermite transform, Signal Process. Image Commun. 28 (3) (2013) 267–291.
[34] S. Sampath, N. Sivaraj, Fuzzy connectedness based segmentation of fetal heart from clinical ultrasound images, in: Advanced Computing, Networking and Informatics, vol. 1, Springer, Cham, 2014, pp. 329–337.
[35] I. Dindoyal, T. Lambrou, J. Deng, A. Todd-Pokropek, Level set snake algorithms on the fetal heart, in: 4th IEEE International Symposium on Biomedical Imaging: From Nano to Macro, 2007 (ISBI 2007), IEEE, Washington, 2007, pp. 864–867.
[36] T.A. Lassige, P. Benkeser, D. Fyfe, S. Sharma, Comparison of septal defects in 2D and 3D echocardiography using active contour models, Comput. Med. Imaging Graph. 24 (6) (2000) 377–388.
[37] Y. Deng, Y. Wang, Y. Shen, P. Chen, Active cardiac model and its application on structure detection from early fetal ultrasound sequences, Comput. Med. Imaging Graph. 36 (3) (2012) 239–247.
[38] C. Goodall, Procrustes methods in the statistical analysis of shape, J. Roy. Stat. Soc. B (1991) 285–339.
[39] C. Solomon, T. Breckon, Fundamentals of Digital Image Processing, Wiley-Blackwell, Chichester, UK, 2011.
[40] T. Cootes, C. Taylor, Constrained active appearance models, in: Proceedings of the Eighth IEEE International Conference on Computer Vision, 2001 (ICCV 2001), vol. 1, 2001, pp. 748–754. vol.1.
[41] T.F. Cootes, C.J. Taylor, On representing edge structure for model matching, in: Proceedings of the IEEE Computer Society Conference on Computer Vision and Pattern Recognition, 2001 (CVPR 2001), vol. 1, IEEE, Hawaii, USA, 2001, pp. I–1114.
[42] I.M. Scott, T.F. Cootes, C.J. Taylor, Improving appearance model matching using local image structure, in: Information Processing in Medical Imaging, Springer, Berlin, Heidelberg, 2003, pp. 258–269.
[43] Y. Ge, D. Yang, J. Lu, B. Li, X. Zhang, Active appearance models using statistical characteristics of Gabor based texture representation, J. Vis. Commun. Image Represent. 24 (5) (2013) 627–634.
[44] P. Kittipanya-ngam, T.F. Cootes, The effect of texture representations on AAM performance, in: 18th International Conference on Pattern Recognition, 2006 (ICPR 2006), vol. 2, IEEE, Hong Kong, 2006, pp. 328–331.
[45] E. Antonakos, J. Alabort-i Medina, G. Tzimiropoulos, S. Zafeiriou, Feature-based Lucas-Kanade and active appearance models, IEEE Trans. Image Process. 24 (9) (2015) 2617–2632.
[46] Y. Su, D. Tao, X. Li, X. Gao, Texture representation in AAM using Gabor wavelet and local binary patterns, in: IEEE International Conference on Systems, Man and Cybernetics, 2009 (SMC 2009), IEEE, USA, 2009, pp. 3274–3279.
[47] S. Ghose, A. Oliver, R. Mart, X. Lladó, J. Freixenet, J.C. Vilanova, et al., Prostate segmentation with texture enhanced active appearance model, in: 2010 Sixth International Conference on Signal-Image Technology and Internet-Based Systems (SITIS), IEEE, Kuala Lumpur, Malaysia, 2010, pp. 18–22.
[48] P.W. Hawkes, Advances in Imaging and Electron Physics, vol. 128, Academic Press, USA, 2003.
[49] J. Carvalho, L. Allan, R. Chaoui, J. Copel, G. DeVore, K. Hecher, et al., ISUOG practice guidelines (updated): sonographic screening examination of the fetal heart, Ultrasound Obstet. Gynecol. 41 (3) (2013) 348–359.
[50] International Society of Ultrasound in Obstetrics & Gynecology, Cardiac screening examination of the fetus: guidelines for performing the “basic” and “extended basic” cardiac scan, Ultrasound Obstet. Gynecol. 27 (1) (2006) 107–113.
[51] V. Damerjian, O. Tankyevych, N. Souag, E. Petit, Speckle characterization methods in ultrasound images—a review, IRBM 35 (4) (2014) 202–213.
[52] B. Wang, D.C. Liu, A novel edge enhancement method for ultrasound imaging, in: 2008 2nd International Conference on Bioinformatics and Biomedical Engineering, 2008, pp. 2414–2417.
[53] S. Queirós, D. Barbosa, B. Heyde, P. Morais, J.L. Vilaça, D. Friboulet, et al., Fast automatic myocardial segmentation in 4D cine CMR datasets, Med. Image Anal. 18 (7) (2014) 1115–1131.
[54] S. Dahdouh, E.D. Angelini, G. Grangé, I. Bloch, Segmentation of embryonic and fetal 3D ultrasound images based on pixel intensity distributions and shape priors, Med. Image Anal. 24 (1) (2015) 255–268.